Journal of Solid State Chemistry 182 (2009) 2646–2655

Contents lists available at ScienceDirect

Journal of Solid State Chemistry

journal homepage: www.elsevier.com/locate/jssc

Processing and characterization of new passive and active oxysulfide glasses in the Ge–Ga–Sb–S–O system

L. Petit [a,*], J. Abel [b], T. Anderson [c], J. Choi [c], V. Nazabal [d], V. Moizan [d], M. Couzi [e], M. Richardson [c], C. Maurel [b], T. Cardinal [b], K. Richardson [a]

[a] School of Materials Science and Engineering, Clemson University, COMSET, 161 Sirrine Hall, Box 340971, Clemson, SC 29634, USA
[b] Institut de Chimie de la Matière Condensée de Bordeaux, CNRS-Université Bordeaux, 87 Av. Dr. Schweitzer, 33608 Pessac, France
[c] CREOL, Center for Research and Education in Optics and Lasers, and College of Optics, University of Central Florida, Orlando, FL 32816, USA
[d] Sciences chimiques de Rennes, UMR-CNRS 6226, Equipe Verres & Céramiques, Université de Rennes 1, Campus de Beaulieu, 35042 Rennes cedex, France
[e] Institut des Sciences Moléculaires, UMR 5255 CNRS, Université Bordeaux 1, 351 Cours de la Libération, 33405 Talence, France

ARTICLE INFO

Article history:
Received 21 May 2009
Received in revised form
19 June 2009
Accepted 11 July 2009
Available online 18 July 2009

Keywords:
Oxysulfide
Raman spectroscopy
Erbium
Luminescence properties
Laser irradiation
Photo-sensitivity

ABSTRACT

New passive and active oxysulfide glasses have been prepared in the Ge–Ga–Sb–S–O system employing a two-step melting process which involves the processing of the chalcogenide glass (ChG) and its subsequent melting with amorphous GeO_2 or Sb_2O_3 powder. Optical characterization of the oxysulfide glasses has shown that the UV cut-off wavelength decreases with increasing oxygen content. Using Raman spectroscopy, correlations have been made between the formation of new Ge- and Sb-based oxysulfide structural units, the Sb content and the O/S ratio. We demonstrate the successful processing of active rare earth doped oxysulfide glasses by melting the chalcogenide glass with Er_2O_3 and Sb_2O_3 and also by melting the Er^{3+} doped chalcogenide glass with Sb_2O_3. Modification of the emission spectra at 1500 nm of Er^{3+} doped samples with the introduction of oxygen revealed that Er^{3+} most likely exists in dual O- and S-neighbor environments. Finally, the photo-response of these new glasses upon near-IR femtosecond laser irradiation has been investigated as a function of Sb content and O/S ratio and shows that the glasses are photo-sensitive to NIR fs laser light with the magnitude of the photo-sensitivity dependent on the glass' Sb content and O/S ratio.

1. Introduction

Recently, there has been a growing research interest in Er^{3+} doped sulfide glasses for the development of planar waveguide and short fiber amplifiers operating at 1.55 and 2.7 μm [1]. The combination of low phonon energy, smaller band gap and high refractive index leads to favorable radiative electron transitions in rare earth (*RE*) ions in sulfide glasses. In the last decade, Er-doped gallium–lanthanum sulfide glasses have been proposed as good candidates for such purposes due to their improved optical properties [2]. However, their applications have been limited by the high photo-sensitivity of chalcogenide glasses (ChGs) to light exposure in the visible and the near-infrared [3]. The proposed effort aims to identify suitably stable compositions with good physical properties throughout the near and mid-infrared (MIR) region, amenable to rare earth doping with minimal photo-sensitivity.

Oxysulfide materials, which are expected to have a better chemical stability upon exposure to visible and NIR light as compared to corresponding sulfide glasses, offer the possibility of combining the mechanical properties of oxide materials with the attractive optical traits of sulfide glasses through adjustment of the sulfur to oxygen ratio. Despite the limited studies on oxysulfide glasses for optical applications, it has been reported in [4] that these newly developed glasses are, also, more resistant to atmospheric attack than corresponding sulfide glasses. Glasses in the La_2O_3–La_2S_3–Ga_2S_3–Ga_2O_3 system have been studied intensively over the last 30 years, for optical applications [5]. More recently, Vila et al. demonstrated the successful processing of Er-containing gallium–lanthanum oxysulfide glasses using Ga_2O_3 and La_2S_3 in a sulfur/argon reactive atmosphere [6]. However, the main drawback to the effective application of sulfide and oxysulfide glasses is the reliance on preparation routes requiring heat treatments in closed systems. Kim et al. [7] have shown that germanium oxysulfide glasses can be prepared in the system $(1-x)GeS_2-xGeO_2$ for $0<x<1$, by rapidly quenching melts to room temperature. We have previously demonstrated that a sulfination heat treatment of GeO_2 powder can be also used to form germanium-based oxysulfide powder [8] resulting in

* Corresponding author.
E-mail address: lpetit@clemson.edu (L. Petit).

0022-4596/$ - see front matter © 2009 Elsevier Inc. All rights reserved.
doi:10.1016/j.jssc.2009.07.020

subsequent oxy-chalcogenide glasses. Thus, it is possible to use these glasses as targets to deposit amorphous films in the GeS_2–GeO_2 system using a radio-frequency (RF) magnetron sputtering technique; this yields a method which offers a fast quenching rate as compared to classical melt quench techniques [8]. More recently, we have reported that oxysulfide bulk glasses can be prepared employing a two-step melting process which involves the processing of the chalcogenide glass (ChG) and its subsequent melting with amorphous oxide powder [9]. This paper aims to extend the study on the processing and characterization of oxysulfide glasses. In this paper, we evaluate the results of effort to prepare new passive and active doped oxysulfide glasses in the Ge–Ga–Sb–S–S system and the impact of mixed chalcogen constituents (O and S) on the resulting physical, optical, structural and luminescence properties of the glasses.

There are few studies involving antimony or germanium oxysulfide glass systems which have been reported [10]. Germanium oxide-based glasses containing heavy metal oxides (Sb_2O_3) have been more widely investigated for IR device applications. Chalcogenides in similar glass systems (Ge–Sb–S) show possible applications as optical transmission media [11]. It has been found that, unlike Ge–Sb–S glasses, Ge–Ga–S glasses are good host materials for incorporation of rare-earths since they have been shown to be capable of dissolving relatively larger amounts of rare-earth elements [12]. Glasses elaborated in the system Ge–Ga–Sb–S present interesting luminescence and nonlinear properties [13,14]. Within this system, fibers, films and rib waveguide doped with rare earth were developed for their attractive fluorescence properties in near and middle-IR [15–17].

In this paper, we present results on the processing and characterization of passive and active oxysulfide glasses in a new system Ge–Sb–Ga–S–O. The sulfide and oxysulfide germanium-based glasses have been prepared with low Sb concentration and with an excess of S to present good physical stability and high nonlinear index suitable for use in novel optical applications. To create a matrix amenable to rare-earth doping in the germanate glass network, a limited fraction of germanium atoms has been replaced by gallium where Ga_2S_3 acts as co-former. The structural changes induced by the addition of oxygen, introduced through melting of amorphous GeO_2 and Sb_2O_3 with glasses in the systems Ge–Sb–S and Ge–Ga–Sb–S, have been systematically investigated using Raman spectroscopy. We also describe how to prepare Er^{3+} doped oxysulfide glasses using undoped chalcogenide and Er^{3+} doped chalcogenide glasses. We discuss the emission spectra of the oxysulfide glasses as a function of the Sb content and O/S ratio. Finally, the response of these new glasses to near-IR femtosecond laser irradiation is also presented and compared as a function of Sb content and S/O ratio.

2. Experimental

Germanium oxysulfide bulk glasses were prepared with different O/S ratios using a two-step melting process in order to determine the maximum concentration of oxygen that can be incorporated without crystallization or phase separation. The first step consisted of the processing of the chalcogenide glass which was then melted, in the second step, with GeO_2 or Sb_2O_3 powder.

The chalcogenide-based glasses in the Ge–Sb–S and Ge–Ga–Sb–S systems were prepared in 20 g batches using high purity elements and compounds (Sb and Ge: Aldrich 99.999%, S: Cerac 99.999% and Ga_2S_3: Aldrich 99.99%). The starting materials were weighed and batched into quartz ampoules inside a nitrogen-purged glove box and sealed under vacuum using a gas–oxygen torch. Prior to sealing and melting, the ampoule and batch were pre-heated at 100 °C for 4 h to remove potential surface moisture from the quartz ampoule and the batch raw materials. The ampoule was then sealed and heated for 24 h at 925 °C. A rocking furnace was used to rock the ampoule and to increase the homogeneity of the melt. Once homogenized, the melt-containing ampoule was air-quenched to room temperature. To avoid fracture of the tube and glass ingot, the ampoules were subsequently returned to the furnace for annealing for 15 h at 40 °C below the glass transition temperature, T_g. The composition of the glasses was analyzed using an Oxford INCAEnergy200 energy dispersive spectroscopy (EDS) system. Within the accuracy of measurements ($\pm 2\%$ for Ge, Ga, Sb, S; $\pm 5\%$ for O), no oxygen was found in the prepared chalcogenide glasses.

The undoped and Er^{3+} doped oxysulfide glasses were prepared by melting in vacuum chalcogenide glasses with GeO_2, Sb_2O_3 or Er_2O_3 powders in graphite crucibles placed inside a quartz ampoule. Due to the small size of the graphite crucible which needs to fit inside the quartz ampoule, only 3 g batches could be prepared. The undoped oxysulfide glasses were prepared by melting the chalcogenide glasses with powder of amorphous GeO_2 (Cerac, 99,999%) and Sb_2O_3 (Aldrich, 99%). Note that for the calculation of the resulting oxysulfide atomic percents, GeO_2 is expressed in molar fraction as $Ge_{33}O_{67}$ and Sb_2O_3 as $Sb_{40}O_{60}$. Four different systems were synthesized: $(1-x)Ge_{23}Sb_7S_{70}-xGe_{33}O_{67}$ with $x=0$ and 0.24; $(1-y)Ge_{23}Sb_7S_{70}-ySb_{40}O_{60}$ with $y=0$, 0.08, 0.15 and 0.22; $(1-x')Ge_{20}Ga_5Sb_{10}S_{65}-x'Ge_{33}O_{67}$ with $x'=0$, 0.14 and 0.26 and finally $(1-y')Ge_{20}Ga_5Sb_5S_{70}-y'Sb_{40}O_{60}$ with $y'=0$, 0.08, 0.17, 0.22. The Er^{3+} doped oxysulfide glasses (5000 weight ppm, corresponding to 5×10^{19} ion/cm^3) were prepared using two techniques:

(i) Melting of Er^{3+} doped Ga-containing chalcogenide glasses with Sb_2O_3.
(ii) Melting of Ga-containing glass with Sb_2O_3 and Er_2O_3 (Aldrich, 99.99%).

The preparation of Er^{3+} doped Ga containing chalcogenide glasses has been described elsewhere [14]. Prior to melting, the ampoule was sealed under vacuum. The melting temperature of 925 °C was reached with a 2.5 °C/min heating ramp without rocking the furnace. After quenching, the oxysulfide glass was removed from the graphite crucible and then annealed in air at 150 °C for 15 h. The oxysulfide glasses were stored in a dry nitrogen environment within a glove box prior to use. The samples were then cut, optically polished and inspected visually.

The glass transition temperature (T_g) was determined by differential scanning calorimetry (DSC) at a heating rate of 10 °C/min from 50 to 500 °C using a commercial apparatus (TA Instruments Inc.). The measurements were carried out in a hermetically sealed aluminum pan. The glass transition temperature was taken at the inflection point of the endotherm, as obtained by taking the first derivative of the DSC curve, and T_g was determined with an accuracy of ± 5 °C. No crystallization temperature was detected up to 500 °C confirming that the investigated glasses are, still, highly stable upon crystallization.

The density of glasses was measured by Archimedes' principle using diethylphtalate as the immersion liquid, with an accuracy of ± 0.02 g/cm^3.

The visible-near infrared (Vis-NIR) absorption spectra were measured at room temperature on 2 mm thick optically polished samples using a Lambda 900 spectrophotometer (Perkin-Elmer Corporation http://www.perkinelmer.com). Fresnel reflections have been subtracted by taking into account that the chalcogenide and oxysulfide glasses exhibit weak absorption around 800 nm.

Raman spectra were recorded at room temperature on a LabRam confocal micro-Raman instrument (Jobin-Yvon), using

Table 1
Nominal and analyzed composition, density, molar volume and glass transition temperature (T_g) of the investigated sulfide and oxysulfide glasses in the Ge–Sb system.

Glass (batch composition)	Composition measured by EDS (±2 at%)	Sb/(S+O)	Density (g/cm^3) (±0.02 g/cm^3)	Molar volume (cm^3/mol) (±0.09 cm^3/mol)	T_g (°C) (±2 °C)
$Ge_{25}Sb_5S_{70}$	$Ge_{25}Sb_7S_{68}$		**2.89**	**16.15**	**343**
$(1-x)Ge_{25}Sb_5S_{70}-xGeO_2$					
$x = 0.24$, $Ge_{27}Sb_4S_{53}O_{16}$	$Ge_{27}Sb_5S_{50}O_{18}$		3.00	14.67	393
$(1-y)Ge_{25}Sb_5S_{70}-ySb_2O_3$					
$y = 0.08$, $Ge_{23}Sb_8S_{64}O_5$	$Ge_{23}Sb_{10}S_{61}O_7$	0.116	2.99	15.97	352
$Ge_{23}Sb_8S_{69}$	$Ge_{23}Sb_8S_{69}$	0.116	**2.94**	**16.52**	**311**
$y = 0.15$, $Ge_{21}Sb_{10}S_{59}O_9$	$Ge_{20}Sb_{11}S_{61}O_9$	0.147	3.10	15.41	327
$Ge_{21}Sb_{10}S_{68}$	$Ge_{21}Sb_{10}S_{68}$	0.147	**3.11**	**15.83**	**305**
$Y = 0.22$, $Ge_{20}Sb_{13}S_{55}O_{13}$	$Ge_{19}Sb_{14}S_{53}O_{14}$	0.191	3.30	15.17	300
$Ge_{20}Sb_{13}S_{67}$	$Ge_{20}Sb_{13}S_{67}$	0.194	**3.25**	**15.95**	**292**

backscattering geometry and a typical resolution of 2–3 cm^{-1}. The system consists of a holographic notch filter for Rayleigh rejection, a microscope equipped with 10×, 50× and 100× objectives (the latter allowing a spatial resolution of less than 2 μm), and a CCD detector. The 752 nm emission line of an argon–krypton laser was used for excitation with incident power of around 10 mW. The use of a 752 nm source was essential to this study because this excitation wavelength was well below the band gap region for most of the studied samples.

The emission spectra in the 1450–1650 nm range were measured at room temperature using an AOC (Applied Optronics Corp.) laser diode excitation source emitting at 980 nm, an Edinburgh Instruments monochromator (M300) and a liquid nitrogen cooled germanium detector (ADC 403L). To compare emission spectra shape as a function of Sb content and O/S ratio, spectra were collected on polished samples. Emission spectrum of Er_2O_3 has been collected on powder between quartz plates.

A custom-made Ti:Al_2O_3 femtosecond laser oscillator was used to study the photo-response of the investigated chalcogenide and oxysulfide glasses to NIR femtosecond laser exposure. The laser produced 100 fs pulses at a 26 MHz repetition rate and a wavelenth of 800 nm. A 0.25NA microscope objective was used to focus the laser light onto the samples, which were mounted on a computer-controlled 3D translation stage (VP-25XA, Newport). The resulting photo-modified surface profile was then analyzed with a white-light interference microscope (Zygo instrument NewView 6300) to assess photo-induced surface modification.

3. Results and discussion

The aim of this study is to investigate the processing and characterization of germanium-based oxysulfide glasses with the compositions $(1-x)Ge_{23}Sb_7S_{70}-xGe_{33}O_{67}$ with $x = 0$ and 0.24; $(1-y)Ge_{23}Sb_7S_{70}-ySb_{40}O_{60}$ with $y = 0$, 0.08, 0.15 and 0.22; $(1-x')Ge_{20}Ga_5Sb_{10}S_{65}-x'Ge_{33}O_{67}$ with $x' = 0$, 0.14 and 0.26 and finally $(1-y')Ge_{20}Ga_5Sb_5S_{70}-y'Sb_{40}O_{60}$ with $y' = 0$, 0.08, 0.17, 0.22 which have been prepared by melting ChG glasses with amorphous GeO_2 or Sb_2O_3 powder. Er^{3+} doped oxysulfide glasses with 5×10^{19} Er^{3+} ions/cm^3 in the Ge–Ga–Sb system have been fabricated by melting undoped chalcogenide glass with Er_2O_3 and Sb_2O_3 and by melting Er^{3+} doped chalcogenide glass with Sb_2O_3. Raman spectroscopy has been employed to track and evaluate structural modifications caused by the systematic substitution of O for S. The luminescence properties of Er^{3+} doped oxysulfide glass have been measured and compared as a function of the Sb/(S+O) ratio. In this paper, we discuss on the evolution of Raman and emission in the 1450–1650 nm range spectral features which are informative of local bonding in the glass network, to understand the correlations between structural characteristics and optical properties of such glasses.

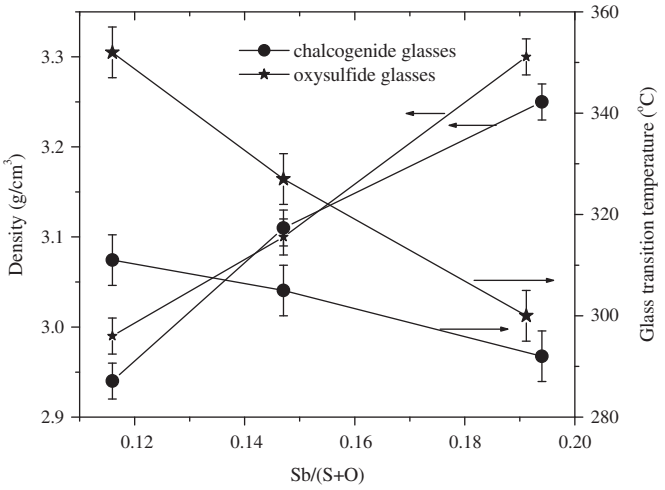

Fig. 1. Density and glass transition temperature as a function of Sb/(S+O) in the Ga-free glasses.

3.1. Effect of oxygen introduction on the structure of gallium-free glasses

Oxysulfide glasses have been obtained by melting the $Ge_{25}Sb_5S_{70}$ glass with amorphous GeO_2 or Sb_2O_3 in a graphite crucible in vacuum. The compositions of the investigated oxysulfide glasses have been determined using EDS. Only one oxysulfide glass could be processed using GeO_2 with homogeneous composition, whereas no issue related to variation in composition has been observed during the processing of the oxysulfide glasses using Sb_2O_3. This is probably due to the different bonding energy of Ge–O and Sb–O dissociation ($E_{\text{bond energy}}$(Ge–O) = 660.3 kJ/mol, $E_{\text{bond energy}}$(Sb–O) = 434 ± 42 kJ/mol) and the chemical affinity of germanium to oxygen [18]. As seen in the oxysulfide glasses in the Ge–As–S–O [9], carbon from the graphite crucible was detected but no clear relation has been observed between the glass composition and carbon content. Table 1 gives the nominal glass compositions and those obtained from the EDS analysis (without considering carbon contamination), the density, molar volume and glass transition temperature of glasses. The density and the glass transition temperature (T_g) increase with the incorporation of GeO_2 in agreement with [9] and have been attributed to the

incorporation of oxygen and probably also to the slight increase of germanium content. Table 1 shows also that the progressive introduction of Sb_2O_3 leads to an increase of the density and a dramatic decrease of the T_g due not only to the partial replacement of sulfur by oxygen but also to the increase of the Sb content. In order to separate the contribution of the S/O ratio change from that of the Sb content increase, chalcogenide glasses have been prepared with the same ratio between the cations than that of the oxysulfide glasses. The density, molar volume and thermal properties of these glasses are also listed in Table 1. Fig. 1 exhibits the change of the density and of the glass transition temperature as a function of ratio Sb/(S+O). In sulfide and oxysulfide, as the ratio Sb/(S+O) rises, the density increases and the T_g decreases. For similar Sb/(S+O) ratio, the replacement of S by O slightly influences the density but strongly increases the glass transition temperature as illustrated in Fig. 1. Such last evolution indicates that stronger bonds have been created confirming the incorporation of oxygen into the glass network.

The absorption spectra of the investigated glasses are shown in Figs. 2a and b. The absorption edge shifts to shorter wavelengths with the introduction of GeO_2 in agreement with our previous study [9], whereas it shifts to longer wavelengths with the addition of Sb_2O_3. Also shown in Fig. 2b are the absorption spectra of the chalcogenide glasses prepared with an excess in Sb content. The increase of the Sb content shifts the absorption band gap to longer wavelengths in agreement with [19], whereas the replacement of S by O induces a shift of the band gap position to shorter wavelength in agreement with [9].

The Raman spectra of the investigated glasses, presented in Figs. 3 and 4, exhibit a broad band with a maximum near 340 cm^{-1} which is formed by the overlap of multiple, contributing Raman signals and smaller bands near 475 cm^{-1}. As a complete

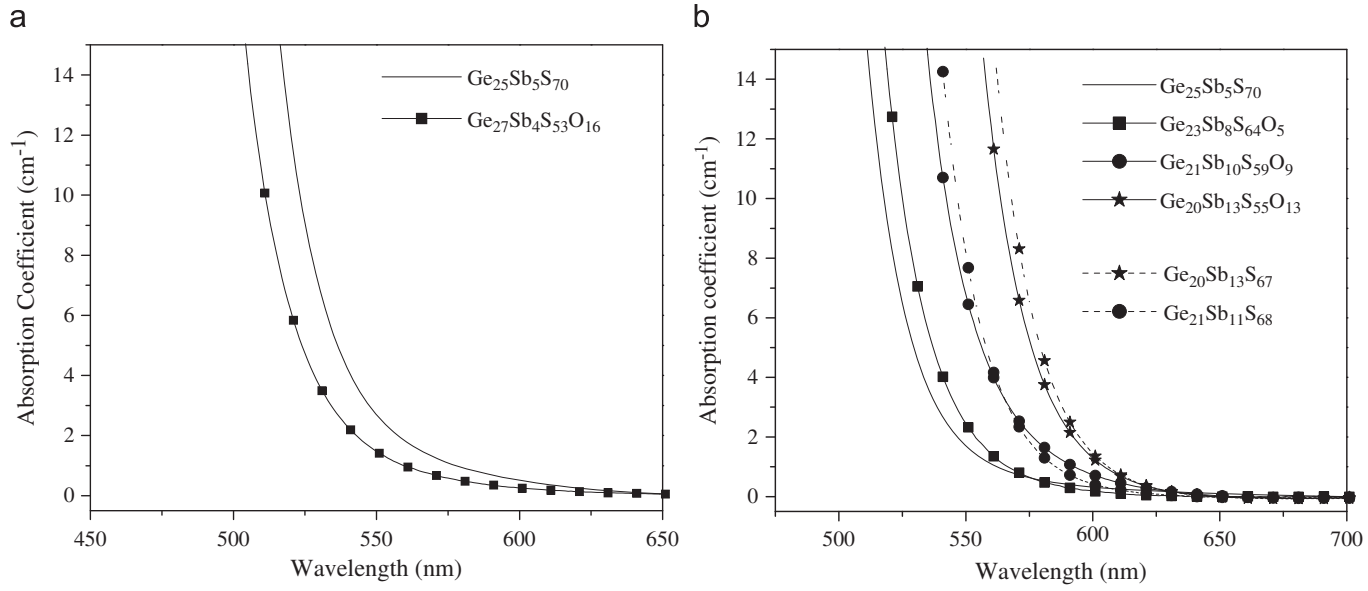

Fig. 2. Absorption spectra of glasses in the systems: $(1-x)Ge_{23}Sb_7S_{70}+xGe_{33}O_{67}$ (a) and $(1-y)\ Ge_{23}Sb_7S_{70}+xSb_{40}O_{60}$ (b).

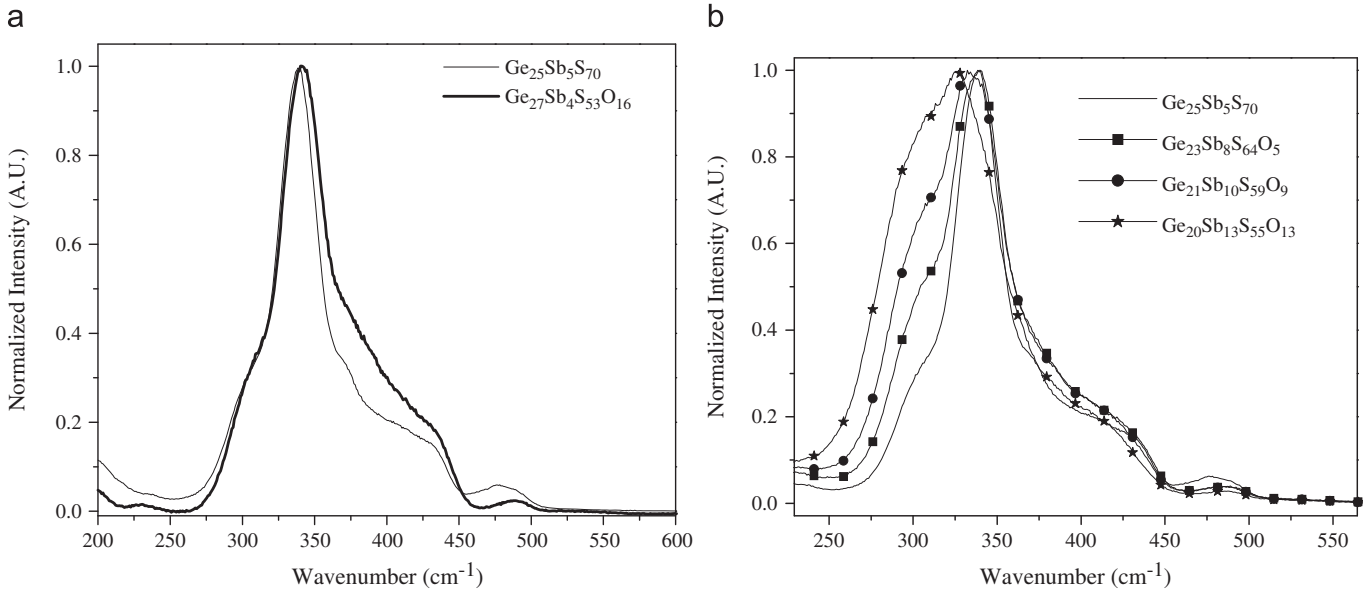

Fig. 3. Raman spectra of glasses in the systems: $(1-x)Ge_{23}Sb_7S_{70}+xGe_{33}O_{67}$ (a) and $(1-y)Ge_{23}Sb_7S_{70}+xSb_{40}O_{60}$ (b).

description of the Raman spectra of a glass with similar composition ($Ge_{23}Sb_7S_{70}$) has been already published in detail in [20], we present here a brief description of the structural characteristics of these glasses. The shoulder at around 300 cm^{-1} has been assigned to the E modes of $SbS_{3/2}$ pyramids. In agreement with [21–24], the bands at 330 and 400 cm^{-1} have been assigned to the A_1 and T_2 modes of corner sharing $GeS_{4/2}$ groups with a smaller contribution of the E mode of the $SbS_{3/2}$ pyramids [25]. The bands at 340, 375 and 420 cm^{-1} have been attributed, respectively to A_1 mode of the GeS_4 molecular units, to the T_2 mode of two edge-sharing $Ge_2S_4S_{2/2}$ tetrahedra and to the vibration of two tetrahedral connected through a bridging sulfur $S_3Ge–S–GeS_3$. The band at 425 cm^{-1} can be attributed to the vibrations of two tetrahedra connected through one bridging sulfur atom, as in $S_3Ge–S–GeS_3$, while the lower intensity band at ca. 475 cm^{-1} may be attributed to the $S_8(A_1)$ ring vibration mode and at 485 cm^{-1} to vibration mode of $S(A_1)$ chain [24].

When GeO_2 is introduced in the $Ge_{25}Sb_5S_{70}$ glass network, the main band becomes broader and shifts to higher wavenumber as seen in Fig. 3a and a new band at ~220 cm^{-1} appears. We attributed these changes to the formation of edge-sharing $GeS_{4/2}$ tetrahedra (shoulder at ca. 375 cm^{-1}) and/or mixed oxysulfide tetrahedral units GeO_3S, GeO_2S_2 or $GeOS_3$ [8,9]. As seen in Fig. 3b, the main band shifts to lower wavenumber with an increase of the

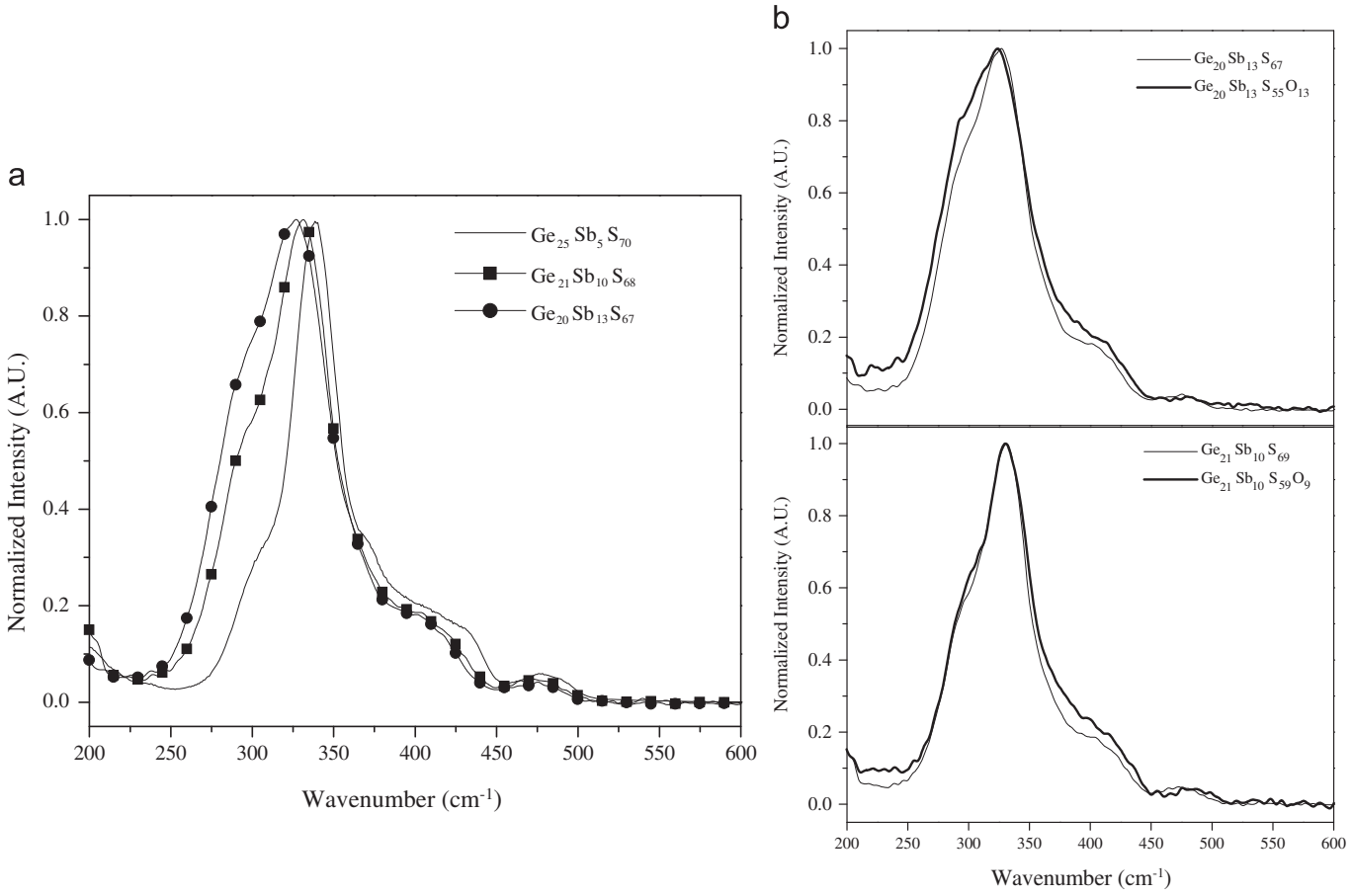

Fig. 4. Raman spectra of the chalcogenide glasses prepared with an excess of Sb glasses (a) and of chalcogenide and oxysulfide glasses with the same Sb/(S+O) ratio (b).

Table 2
Nominal and analyzed composition, density, molar volume and glass transition temperature (T_g) of the investigated sulfide and oxysulfide glasses in the system Ge–Ga–Sb system.

Glass (batch composition)	Composition measured by EDS (±2%)	Sb/(S+O)	Density (g/cm^3) (±0.02 g/cm^3)	Molar volume (cm^3/mol) (±0.09 g/cm^3)	T_g (°C) (±2 °C)
$(1-x')Ge_{20}Ga_5Sb_{10}S_{65}–x'GeO_2$					
$Ge_{20}Ga_5Sb_{10}S_{65}$	$Ge_{20}Ga_5Sb_{10}S_{65}$		**3.25**	**15.70**	**321**
$x' = 0.14$, $Ge_{22}Ga_4Sb_9S_{56}O_9$	$Ge_{20}Ga_5Sb_{10}S_{55}O_{10}$		3.27	15.02	339
$x' = 0.26$, $Ge_{23}Ga_4Sb_7S_{48}O_{17}$	$Ge_{20}Ga_4Sb_9S_{50}O_{17}$		3.28	14.06	343
$(1-y')Ge_{20}Ga_5Sb_5S_{70}–y'Sb_2O_3$					
$Ge_{20}Ga_5Sb_5S_{70}$	$Ge_{20}Ga_5Sb_5S_{70}$		**2.91**	**15.99**	**316**
$y' = 0.08$, $Ge_{18}Ga_5Sb_8S_{64}O_5$	$Ge_{17}Ga_4Sb_{10}S_{63}O_6$	0.116	3.05	15.61	327
$Ge_{18}Ga_5Sb_8S_{69}$	$Ge_{18}Ga_5Sb_8S_{69}$	**0.116**	**3.06**	**15.82**	**300**
$y' = 0.17$, $Ge_{17}Ga_4Sb_{11}S_{58}O_{10}$	$Ge_{16}Ga_4Sb_{12}S_{58}O_9$	0.162	3.27	14.90	313
$Ge_{17}Ga_4Sb_{11}S_{68}$	$Ge_{17}Ga_4Sb_{11}S_{68}$	**0.162**	**3.25**	**15.48**	**287**
$y' = 0.22$, $Ge_{16}Ga_3Sb_{13}S_{55}O_{13}$	$Ge_{16}Ga_4Sb_{12}S_{55}O_{12}$	0.194	3.36	14.66	304
$Ge_{16}Ga_3Sb_{13}S_{67}$	$Ge_{16}Ga_3Sb_{13}S_{67}$	**0.194**	**3.38**	**15.09**	**283**

shoulder amplitude at 300 cm^{-1} with the progressive incorporation of Sb_2O_3 in the germanate network. Similar variations in the Raman spectra of the chalcogenide glasses can be observed in Fig. 4a as the Sb content rises. These variations indicate an increase of the SbS_3 units and consequently a decrease of the $GeS_{4/2}$ units and of the Ge–S–Ge bonds in the glass network. In Fig. 4b are the Raman spectra of oxysulfide and chalcogenide glasses with similar Sb/(S+O) ratio. In both spectra, the replacement of sulfur by oxygen leads to an increase of the shoulder in the 350–450 cm^{-1} range and at ~300 cm^{-1}. These variations are more pronounced for larger content of Sb and O. As performed elsewhere [8,9], the main band could not be obtained by simple summation of GeS_2 vibrational features to the oxide spectra. The addition of new bands between 360 and 400 cm^{-1}, different from GeO_4 or GeS_4 tetrahedral sites, and at ~320 cm^{-1}, different from SbO_3 and SbS_3 units, was necessary to correctly simulate the spectrum. We observed that the intensity of the band in the 360–400 cm^{-1} range increases with an increase of O content while the amplitude of the band at 320 cm^{-1} increases not only with an increase of O content but also with an increase of Sb content. In agreement with [8], the first band can be attributed to the presence of changes to the formation of edge-sharing $GeS_{4/2}$ tetrahedra (shoulder at ca. 375 cm^{-1}) and/or mixed oxysulfide tetrahedral units GeO_3S, GeO_2S_2 or $GeOS_3$. As the Sb content is large in these oxysulfide glasses, the second new contribution in the Raman spectra might be related to the formation of species such as SbO_2S or $SbOS_2$ units.

In summary, the Raman spectra show that introduction of GeO_2 or Sb_2O_3 in the Ge–Sb–S glass induces changes in the interconnectivity of GeS_4 tetrahedra due to variations in the sulfur content, leading probably to the formation of new oxysulfide units such as $GeOS_3$, GeO_2S_2 or GeO_3S and probably SbO_2S or $SbOS_2$ units in high Sb concentrated glasses. These structural changes are consistent with the blue-shift of the absorption edge observed in Figs. 2a and b and the increase of T_g (Table 1 and Fig. 1).

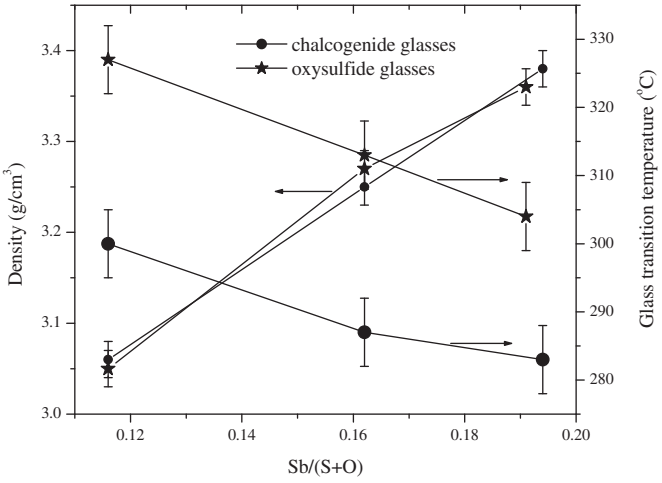

Fig. 5. Density and glass transition temperature as a function of Sb/(S+O) in the Ga-containing glasses.

3.2. *Effect of oxygen introduction on the structure of gallium-containing glasses*

Table 2 summarizes the density, molar volume and T_g of the investigated gallium-containing oxysulfide glasses prepared by adding GeO_2 and Sb_2O_3 in the Ge–Ga–Sb–S glass. As seen in the gallium-free system (Table 1), the incorporation of GeO_2 leads to an increase of the density and T_g and a decrease of the molar volume, whereas the progressive introduction of Sb_2O_3 induces a decrease of the T_g and molar volume and an increase of the density. As performed in the other glass system, chalcogenide glasses have been prepared with the same ratio between the cations than that of the oxysulfide glasses. An increase of the Sb content leads to an increase of the density and to a decrease of the T_g, whereas the replacement of sulfur by oxygen leads only to an increase of the T_g. The variation in density due to the replacement of sulfur by oxygen is less distinct as seen in Fig. 5. However, the T_g of the oxysulfide glasses is much larger than that of the corresponding chalcogenide glasses for similar Sb/(S+O) ratio confirming the incorporated of oxygen in the sulfide network.

Figs. 6a and b exhibit the absorption spectra of the glasses. Similar changes of the absorption edge position with the addition of GeO_2 and Sb_2O_3, with the increase of the Sb content and with the progressive replacement of sulfur by oxygen than those observed in Figs. 2a and b can be observed. However, compared to the absorption spectra shown in Figs. 2a and b, the absorption

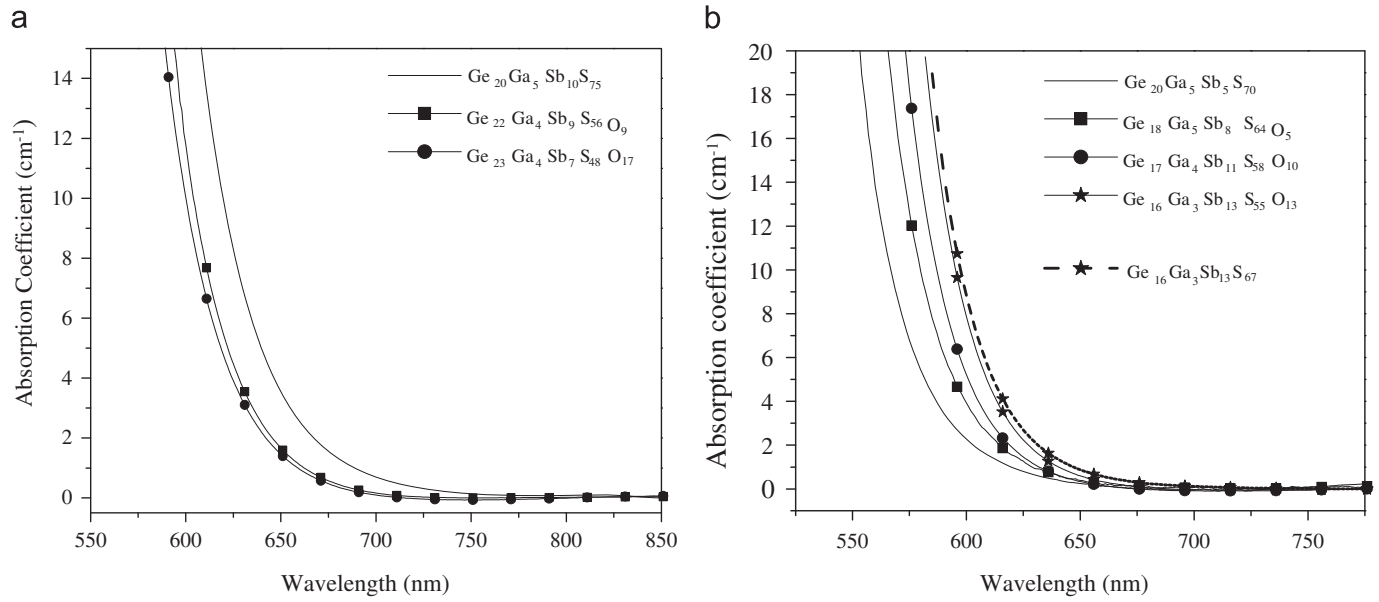

Fig. 6. Absorption spectra of glasses in the systems: $(1-x')Ge_{20}Ga_5Sb_{10}S_{65}-x'GeO_2$ (a) and $(1-y')Ge_{20}Ga_5Sb_5S_{70}-y'Sb_2O_3$ (b).

band gap is less shifted to lower wavelength when sulfur is replaced by the same amount of oxygen.

The Raman spectra of new glasses are presented in Fig. 7. As explained elsewhere [26], gallium is expected to be organized in $GaS_{4/2}$ tetrahedral units connected through bridging sulfur atoms in the germanate network within the Ge–Ga–Sb–S glasses. Compared to the Raman spectra in Figs. 3a and b, the main band is broader as the frequencies of the fundamental vibration modes of $GaS_{4/2}$ units are very close to those of $GeS_{4/2}$ tetrahedra [27]. As seen in Figs. 3a and b, the introduction of GeO_2 leads to a shift of the main band to higher wavenumber, whereas the progressive addition of Sb_2O_3 leads to a shift of the main band to lower wavenumber. Fig. 7c exhibits the Raman spectra of an oxysulfide glass and of a sulfide glass with the same Sb/(S+O) ratio at 0.162, taken as an example. The replacement of sulfur by oxygen leads to similar but less distinct variations in the Raman signal than those seen in Fig. 4b indicating less structure variation. Gallium containing glasses seem to offer better ability to incorporate oxygen without strong change of the sulfide glass network in agreement with the small blue shift of the absorption band gap seen in Fig. 6b.

Rare earth doped oxysulfide glasses have been prepared by melting $Ge_{20}Ga_5Sb_5S_{70}$ with Sb_2O_3 and Er_2O_3 and also by melting Er^{3+} doped $Ge_{20}Ga_5Sb_{10}S_{65}$ with Sb_2O_3 using the process detailed in the experimental paragraph. No absorption band related to the *4f–4f* transitions of Er^{3+} could be observed in the absorption spectrum of the oxysulfide glasses on 1 mm thick sample indicating that all Er^{3+} ions have not been introduced in the oxysulfide network. Nevertheless, fluorescence around 1.5 μm was obtained in these oxysulfide glasses with an excitation at 980 nm. Fig. 8a shows the emission spectra of the Er^{3+} doped $Ge_{20}Ga_5Sb_{10}S_{65}$ glass and of the same glass melted with Sb_2O_3. The fluorescence band which corresponds to the transition from the $^4I_{13/2}$ level to $^4I_{15/2}$ level of Er^{3+}, present classical shape for the Er^{3+} doped $Ge_{20}Ga_5Sb_{10}S_{65}$ sample [16]. It is clearly shown that the two glasses exhibit different emission spectra demonstrating that the melting of the chalcogenide glass with Sb_2O_3 induces significant changes in the rare earth environment which is in

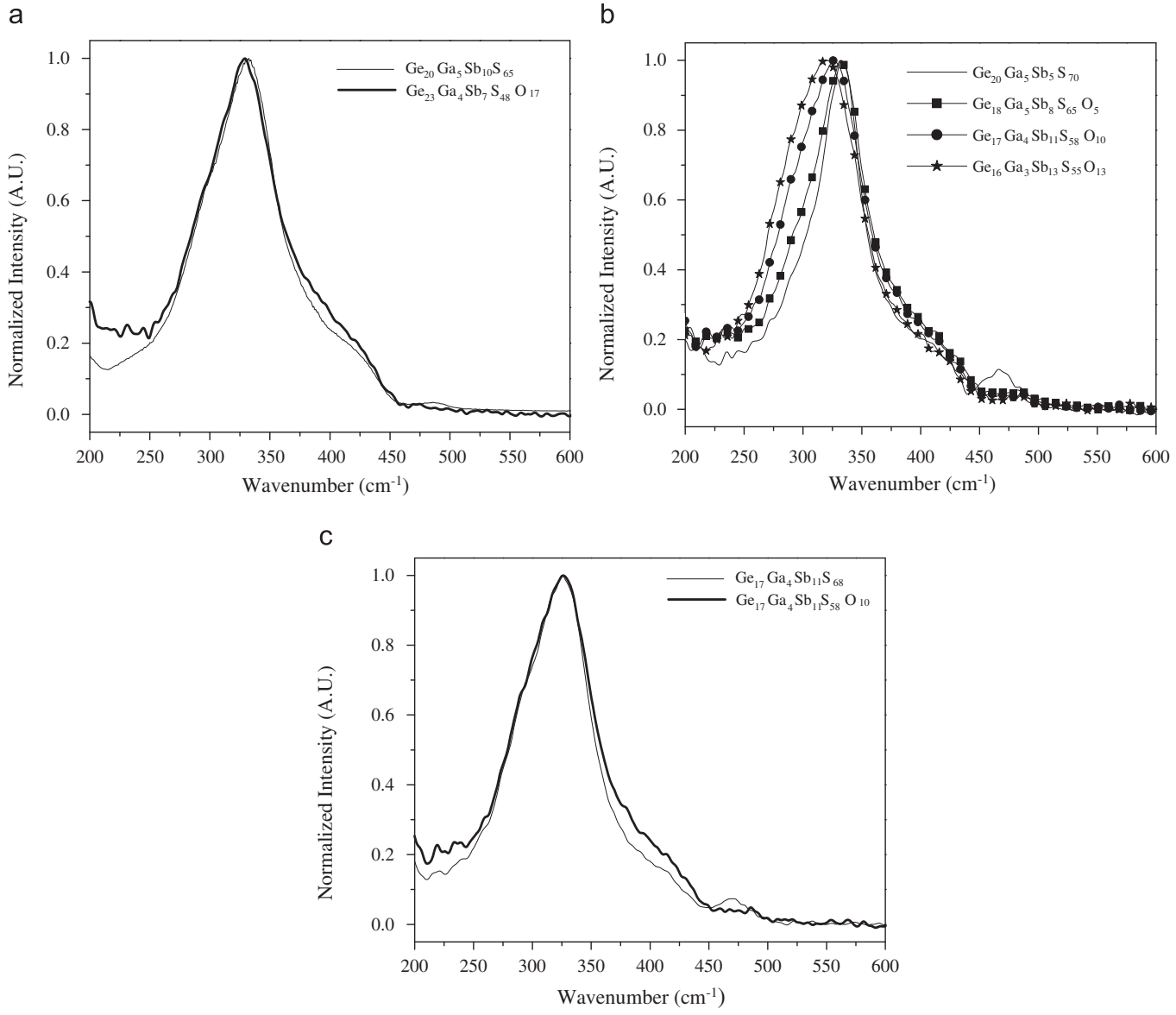

Fig. 7. Raman spectra of glasses in the systems: $(1-x')Ge_{20}Ga_5Sb_{10}S_{65}-x'GeO_2$ (a), $(1-y')Ge_{20}Ga_5Sb_5S_{70}-y'Sb_2O_3$ (b) and of the chalcogenide and the oxysulfide glasses with the Sb/(S+O) ratio equal to 0.162.

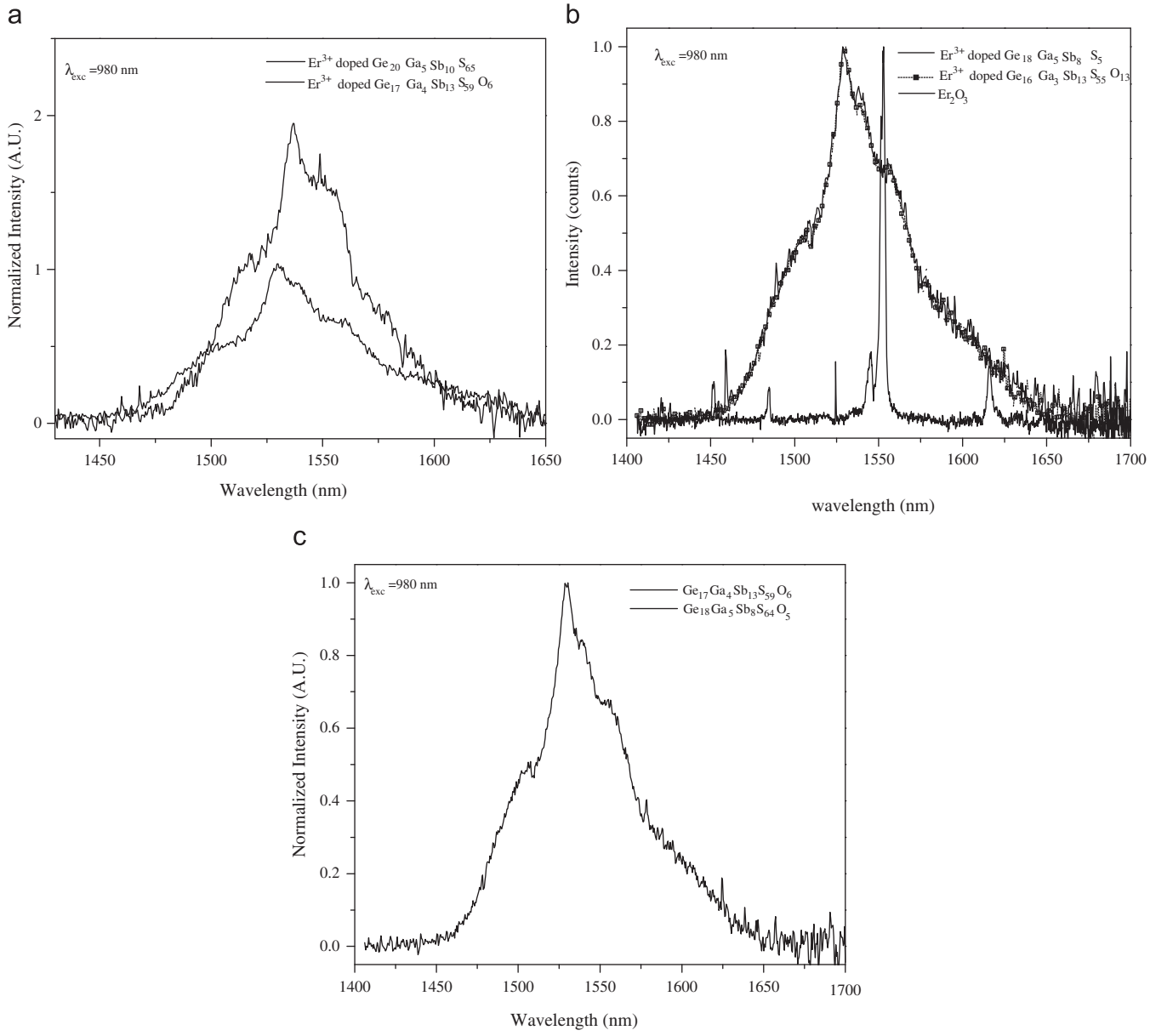

Fig. 8. Emission spectra after excitation at 980 nm of Er^{3+} doped $Ge_{20}Ga_5Sb_{10}S_{65}$ glass and the Er^{3+} doped $Ge_{17}Ga_4Sb_{13}S_{59}O_6$ glass (a): of two Er^{3+} doped OChG glasses and of Er_2O_3 (b) and of Er^{3+} doped $Ge_{17}Ga_4Sb_{13}S_{59}O_6$ glass (melting of Er^{3+} doped $Ge_{20}Ga_5Sb_{10}S_{65}$ glass with Sb_2O_3) and of Er^{3+} doped $Ge_{18}Ga_5Sb_8S_{64}O_5$ glass (melting $Ge_{20}Ga_5Sb_5S_{70}$ with Sb_2O_3 and Er_2O_3).

agreement with the structure variation seen in Figs. 7a and b. The bandwidth of the emission band of the chalcogenide glass was measured at 51 nm while it was measured at 57 nm for the oxysulfide glass indicating that the 4*f* levels in the oxysulfide network are further split or that stronger inhomogeneous broadening is occurring due to multiple erbium sites. This is indicative or proximity of erbium ions near both oxygen and sulfur species in the network. Other active oxysulfide glasses have been, also, processed by melting the $Ge_{20}Ga_5Sb_7S_{70}$ glass with Er_2O_3 and Sb_2O_3. Fig. 8b presents the emission spectra of these new Er^{3+} doped oxysulfide glasses as a function of the Sb_2O_3 content. The spectra exhibit a broad band corresponding to the transition from the $^4I_{13/2}$ level to $^4I_{15/2}$ level of Er^{3+} with some sharp peaks which do not correspond to the luminescence of Er^{3+} in Er_2O_3 as seen in Fig. 8b. The attribution of these sharp emission peaks is still not understood and is under investigation. The measurement of a broad emission reveals that a large content of Er^{3+} ions are located in an amorphous matrix. An increase of the Sb_2O_3 content leads to a small increase of the shoulders amplitude at ~1538 and 1550 nm indicating that the site of Er^{3+} is sensitive to the incorporation of Sb_2O_3. Fig. 8c compares the emission spectra of oxysulfide glasses prepared by melting (i) $Ge_{20}Ga_5Sb_5S_{70}$ with Sb_2O_3 and Er_2O_3 and (ii) Er^{3+} doped $Ge_{20}Ga_5Sb_{10}S_{65}$ with Sb_2O_3. The glasses have equivalent S/O ratio but different molar fractions of Sb. It is clearly shown that the emission spectra are similar with some variation in amplitude of the shoulders at ~1538 and 1550 nm indicating that the significant variations in the emission spectra observed in Fig. 8a with the incorporation of Sb_2O_3 are thought to be mainly due to the incorporation of oxygen in the site of Er^{3+}. The measurement of the luminescence properties of the active oxysulfide glasses confirms the presence of oxygen and sulfur around erbium ions which lead to strong spectral change from sulfide to oxysulfide composition. The small changes in Fig. 8c can be related to slight variation of antimony content around the Er^{3+} ions.

3.3. Photo-induced material modification with a near-IR femtosecond laser irradiation

Lastly, the photo-response of the oxysulfide glasses to near-IR femtosecond laser irradiation has been studied as a function of Sb content and O/S ratio in order to determine the potential for fabricating optical elements in these glasses through direct femtosecond laser direct writing. We have first determined the threshold between ablation and photo-induced modification by independently increasing the laser intensity and number of pulses until ablation was observed. The threshold for the onset of ablation as compared to nonablative photo-modification was determined by irradiated separate spots with a specific number of pulses, followed by incrementally increasing the laser intensity resulting in a two-dimensional map. It is interesting to point out that as seen in the glasses in the similar Ge(Ga)–Sb–S(Se) system [28–30], the ablation threshold was found to be not only a function of the laser intensity but also of the accumulated number of laser shots per focal spot. The sample surface was found to be more sensitive to the laser intensity than to the number of pulses independent of the Sb content and S/O ratio. Table 3 summarizes the ablation threshold of some of the investigated chalcogenide and oxysulfide glasses using 4×10^6 pulses per focal spot at a repetition rate of 26 MHz. The ablation threshold decreases progressively with an increase of the Sb content in agreement with the shift of the absorption band gap to larger wavelength as seen in Fig. 2b. The oxysulfide glass exhibits a similar ablation threshold than that of the chalcogenide glass with the same Sb/(S+O) ratio, probably due to the small shift of the absorption band gap to shorter wavelength when sulfur is replaced by oxygen as explained previously.

Table 3
Ablation threshold of sulfide and oxysulfide glasses.

Glass (batch composition)	Ablation threshold using 4×10^6 pulses per focal spot (GW/cm^2) ($\pm$10%)
$Ge_{23}Sb_8S_{64}O_5$	106.0
$Ge_{21}Sb_{10}S_{59}O_9$	84.2
$Ge_{21}Sb_{10}S_{68}$	**66.2**
$Ge_{20}Sb_{13}S_{55}O_{13}$	72.3
$Ge_{20}Sb_{13}S_{67}$	**80.4**

When irradiated with a laser intensity at 90% of their respective ablation thresholds as defined and discussed in detail for other bulk and thin film exposure studies in [28–30], surface photo-expansion was observed. The glasses were irradiated with a laser intensity at 90% of their respective ablation threshold using various number of pulses. Figs. 9a and b show the surface photo-expansion of, respectively, the chalcogenide and oxysulfide glasses as a function of the number pulses incident on the material per focal spot. The surface photo-expansion depends on the number of pulses and on the composition of the glass as observed in our prior works on glasses in the Ge(Ga)–Sb–S(Se) in [28–30]. The surface photo-expansion increases with an increase of the number of pulses probably due to an increased coupling of the laser energy to the glass matrix through cumulative heating. The oxysulfide glasses exhibit lower surface photo-expansion than the chalcogenide glasses. Moreover, we can notice that the chalcogenide glass with the highest Sb content exhibits the largest surface photo-expansion, whereas the oxysulfide glass with the highest Sb content which is also the most concentrated in oxygen has the lowest surface photo-expansion. Using micro-Raman spectroscopy, we related the surface photo-expansion of the glasses in the system $Ge_{23}Sb_7S_{70-x}Se_x$ to modification of bonding forms under laser irradiation and reorganization of the glass structural units [30]. We showed that the near-surface photo-expansion can be related to an increased connection of GeS_4 units to form corner sharing $GeS_{4/2}$ units with a concurrent formation of S–S bridges. The introduction of Se in the germanate network was found to restrict the connection between GeS_4 units through S–S bridges after laser irradiation leading to smaller surface photo-expansion. In the present study, it is possible to think that the presence of oxygen and the enhanced average bond strength of the mixed chalcogen network may also restrict the reorganization of the glass' structural units leading to a smaller surface photo-expansion with the same exposure dose. A complete study on the effect of the laser exposure on the structure of the oxysulfide glass will be published separately.

4. Conclusions

A two-step melting process has been developed to obtain new oxysulfide glasses by melting a glass in the Ge–Ga–Sb–S system

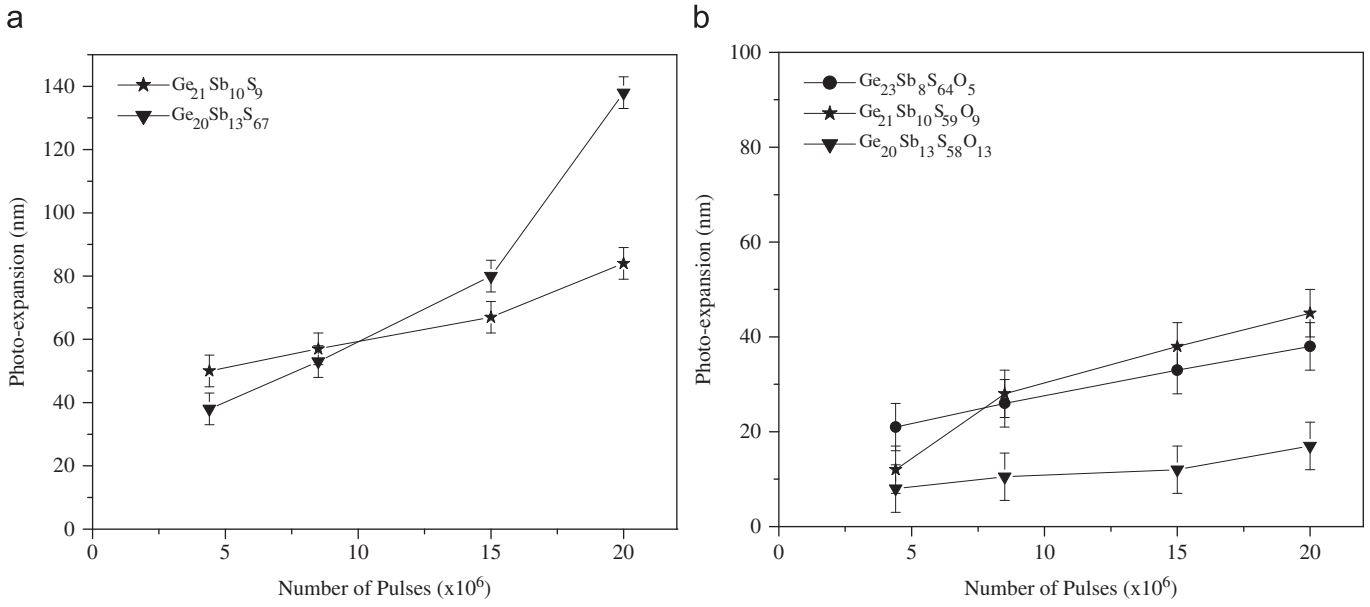

Fig. 9. Surface photo-expansion of the chalcogenide (a) and oxysulfide (b) glasses as a function of the number of pulses per focal spot incident on the glass.

with GeO_2 or Sb_2O_3 powder. We have shown that an increase of oxygen content decreases the UV cut-off wavelength seen for the oxygen-free chalcogenide glass and increases the glass transition temperature, T_g, due to an increase in the average network former bond strength. Successful processing of Er^{3+} doped oxysulfide glasses has been demonstrated using two melt processing techniques: the remelt of the chalcogenide glasses with Er_2O_3 and Sb_2O_3 or the remelt of a Er^{3+} doped chalcogenide with Sb_2O_3. The resulting oxysulfide glasses were found to have a similar emission band at around 1500 nm when excited at 980 nm. The compositional dependence of the Raman and emission at 1.5 μm spectra suggests the presence of the formation of mixed Ge-, Sb- and Er-based oxysulfide units including Er^{3+} ions neighboring both S and O species. Finally, we have demonstrated that these new oxysulfide glasses are photo-sensitive to near-IR femtosecond laser irradiation and exhibit a surface photo-expansion after laser irradiation which remains, as expected, lower than similar response seen for oxygen-free chalcogenide glasses.

Acknowledgments

This work has been supported by the National Science Foundation international Grants EEC-0244109 and DMR-031208. Support was also provided by educational US and French grants, including the Agence Nationale de la Recherche (Grant ANR-05-BLAN-0212-01), the CNRS (PICS Grant 3179) and a FACE Grant from the French Embassy in the US. Partial support from the EC through the Marie Curie Actions—NANONLO project (MTKD-CT-2006-042301) is also acknowledged.

References

[1] J.A. Medeiros Neto, E. Taylor, B. Samson, J. Wang, D.W. Hewak, Journal of Non-Crystalline Solids 184 (1995) 292.
[2] K. Wei, D.P. Machewirth, J. Wenzel, E. Snitzer, G.H. Sigel, Journal of Non-Crystalline Solids 182 (1995) 257.
[3] D. Savastru, S. Miclos, R. Savastru, Journal of Optoelectronics and Advanced Materials 8 (2006) 1165–1172.
[4] P.N. Kumta, S.H. Risbud, Ceramic Bulletin 69 (1990) 1977.
[5] L.G. Hwa, J.G. Shiau, S.P. Szu, Journal of Non-Crystalline Solids 249 (1999) 55.
[6] L.D. Vila, N. Aranha, Y. Messaddeq, E.B. Stucchi, S.J.L. Ribeiro, D. Fagundes, L.A.O. Nune, Journal of Alloys and Compounds 344 (2002) 226–230.
[7] Y. Kim, J. Saienga, S.W. Martin, Journal of Non-Crystalline Solids 351 (2005) 1973–1979.
[8] C. Maurel, T. Cardinal, P. Vinatier, L. Petit, K. Richardson, F. Guillen, M. Lahaye, M. Couzi, F. Adamietz, V. Rodriguez, M. Bellec, L. Canioni, Materials Research Bulletin 43 (2008) 1179–1187.
[9] C. Maurel, L. Petit, M. Dussauze, E.I. Kamitsos, M. Couzi, T. Cardinal, A.C. Miller, H. Jain, K. Richardson, Journal of Solid State Chemistry 181 (2008) 2869–2876.
[10] E.F. Riebling, Journal of Materials Science 9 (1974) 753.
[11] A. Znobrik, J. Stetzif, I. Kavich, V. Osipenko, I. Zachko, N. Balota, O. Jakivchuk, Ukrainian Journal of Physics 26 (1981) 212.
[12] Z.G. Ivanova, V.S. Vassilev, E. Cernoskova, Z. Cernosek, Journal of Physics and Chemistry of Solids 64 (2003) 107–110.
[13] M. Guignard, V. Nazabal, F. Smektala, J.L. Adam, O. Bohnke, C. Duverger, A. Moréac, H. Zeghlache, A. Kudlinski, G. Martinelli, Y. Quiquempois, Advanced Functional Materials 17 (2007) 3284–3294.
[14] Y. Guimond, J.-L. Adam, A.-M. Jurdyc, H.L. Ma, J. Mugnier, B. Jacquier, Journal of Non-Crystalline Solids 256–257 (1999) 378–382.
[15] M. De Sario, L. Mescia, F. Prudenzano, F. Smektala, F. Deseveday, V. Nazabal, J. Troles, L. Brilland, Optics & Laser Technology 41 (2009) 99–106.
[16] V. Moizan, V. Nazabal, J. Troles, P. Houizot, J.-L. Adam, F. Smektala, G. Gadret, S. Pitois, J.-L. Doualan, R. Moncorgé, G. Canat, Optical Materials 31 (2008) 39–46.
[17] V. Nazabal, P. Nemec, J. Jedelsky, C. Duverger, J. Le Person, J.L. Adam, M. Frumar, Optical Materials 29 (2006) 273–278.
[18] R.C. Weast, M.J. Astle, CRC Handbook of Chemistry and Physics, sixty first ed., CRC Press, Boca Raton, 1980–1981 pp. D-68–D-71..
[19] L. Petit, N. Carlie, K.C. Richardson, M. Couzi, F. Adamietz, V. Rodriguez, Materials Chemistry and Physics 97 (2006) 64–70.
[20] L. Petit, N. Carlie, K. Richardson, Y. Guo, A. Schulte, B. Campbell, B. Ferreira, S. Martin, Journal of Physics and Chemistry of Solids 66 (2005) 1788–1794.
[21] G. Lucovsky, F.L. Galeener, R.C. Keezer, R.H. Geils, H.A. Six, Physical Review B 10 (1974) 5134–5146.
[22] K. Murase, T. Fukunaga, Y. Tanaka, K. Yakushiji, I. Yunoki, Physica B 117–118 (1983) 962–964.
[23] P. Boolchand, J. Grothaus, M. Tenhover, M.A. Hazle, R.K. Grasselli, Physical Review B 33 (1986) 5421–5434.
[24] E.I. Kamitsos, J.A. Kapoutsis, G.D. Chryssikos, G. Taillades, A. Pradel, M. Ribes, Journal of Solid State Chemistry 112 (1994) 255–261.
[25] B. Frumarova, P. Nemec, M. Frumar, J. Oswald, M. Vleck, Journal of Non-Crystalline Solids 256–257 (1999) 266–270.
[26] J. Heo, J.M. Yoon, S.Y. Ryou, Journal of Non-Crystalline Solids 238 (1998) 115–123.
[27] L. Koudelka, M. Pisarcik, O.L. Baidakova, Journal of Materials Science Letters 8 (1989) 1161–1162.
[28] L. Petit, J. Choi, T. Anderson, R. Villeneuve, J. Massera, N. Carlie, M. Couzi, M. Richardson, K. Richardson, Optical Materials 31 (2009) 965–969.
[29] T. Anderson, L. Petit, N. Carlie, J. Choi, J. Hu, A. Agarwal, L. Kimerling, K. Richardson, M. Richardson, Optics Express 16 (24) (2008) 20081–20098.
[30] L. Petit, N. Carlie, T. Anderson, M. Couzi, J. Choi, M. Richardson, K. Richardson, Optical Materials 29 (2007) 1075–1083.